Iran J Sci Technol Trans Electr Eng
DOI 10.1007/s40998-017-0023-7

RESEARCH PAPER

An Analytical Fifth-Nearest Neighbor Tight-Binding Investigation of the Effect of Mechanical Deformations on SWCNTs

Mehdi Pakkhesal[1] · **Seyed Ebrahim Hosseini**[1]

Received: 17 November 2016 / Accepted: 19 June 2017

Abstract In this paper, we analytically investigate the effects of the two samples of mechanical deformations, i.e., uniaxial and torsional strains on the electronic band structure and the density of states of the single-walled carbon nanotubes (SWCNTs) using the nearest neighbor, the third-nearest neighbor (3-NN-TB) and the fifth-nearest neighbor tight-binding (5-NN-TB) approaches to compare the estimated band gap and the density of states of the three methods. To do this, we not only make use of the previous works but also analytically develop a 5-NN-TB-based model for the investigation of the mentioned types of strains. The purpose of this paper is to employ this model for the investigation of the two types of strain in order to acquire an analytic formula for the band structure under strain and get the advantage of analytic formula (e.g., speed in band structure calculations under strain) in conjunction with the high degrees of accuracy.

keywords Density of states · Single wall CNT · Tight binding · Mechanical deformation · Band structure

1 Introduction

Semiconductors are the basic elements of today's electronic devices which can transport the electronic carriers in a controlled manner, detect light emissions, emit light and so on. But nearly all of their electronic properties depend on their electronic band structure, band gap and the density of states (DOS). These characteristics of semiconductors are in turn subject to the changes due to dozens of phenomena, e.g., temperature, mechanical strains. On the other hand, carbon nanotubes are the rather new types of semiconductors. Their electronic properties have been investigated since the time of their exploration (Saito et al. 1992; Zang 2005; Wan-Sheng 2013; Bahari and Amiri 2012; Sivasathya and Thiruvadigal 2013; Souier et al. 2013). From here on, we theoretically develop a fifth-nearest neighbor π-tight-binding model for the investigation of the effects of the two types of mechanical strains and then compare it with the results of the nearest neighbor and the third-nearest neighbor tight-binding approaches. The problem of the effect of uniaxial and torsional strains on band gap is originally claimed by Yang et al. (1999) who treated the problem by the nearest neighbor tight-binding model, which is first used by Saito et al. (1992) to treat SWCNTs in non-strained mode. In 2002, the band structure of SWCNTs (in the absence of strain) was treated with the third-nearest neighbor tight model by Reich et al. (2002) as more accurate and closer results to ab initio results. However, this problem was once again treated using the fifth-nearest neighbor tight-binding approximation by Han et al. (2010). They also showed that their results are ten times closer to the ab initio results than that of (Reich et al. 2002), i.e., in this situation the maximal deviation of the corresponding TB approximation from the first-principle calculation is 0.025 eV while it is 0.25 eV for MΓKM (all $\boldsymbol{k}$'s along high symmetry lines) in its 3-NN-TB (third-nearest neighbor tight binding) counterpart. In the following lines, we develop a perturbed 5-NN-TB in order to estimate the response to the mentioned types of

✉ Seyed Ebrahim Hosseini
ehosseini@um.ac.ir

Mehdi Pakkhesal
pakkhesal.mehdi@mail.um.ac.ir

[1] Department of Electrical Engineering, Ferdowsi University of Mashhad, Mashhad, Iran

Published online: 21 July 2017

strains. Next, in Sect. 3, we compare the results with the nearest and the third-nearest neighbor tight-binding approximations.

2 Method

As is known theoretically, SWCNT can be considered as a graphene sheet that is rolled over into a cylinder on a lattice vector $\boldsymbol{C}$ so that the beginning and the end of $\boldsymbol{C}$ join together. Illustrated in Fig. 1 is the graphene sheet with the lattice vector $\boldsymbol{C}$ and the unit lattice vectors $\vec{a}_1$ and $\vec{a}_2$. The nearest, the second-nearest, the third-nearest and the fifth-nearest neighbors are also illustrated in this figure.

According to Fig. 1 $= n_1\vec{a}_1 + n_2\vec{a}_2$, where $a = |\vec{a}_1| = |\vec{a}_2| = \sqrt{3}a_{\mathrm{C-C}}$, being $a_{\mathrm{C-C}}$ carbon–carbon bonding distance in the absence of strain, which is 0.142 nm and $|\boldsymbol{C}| = ac_h = a\sqrt{n_1^2 + n_2^2 + n_1 n_2}$. Now, let the unit vectors $\hat{c} = \frac{\boldsymbol{C}}{|\boldsymbol{C}|}$ and $\hat{t} = \frac{\boldsymbol{T}}{|\boldsymbol{T}|}$, where $\mathbf{T}$ is the one-dimensional lattice vector (White et al. 1993) which is perpendicular to vector $\boldsymbol{C}$, we find that:

$$\hat{c} = \frac{n_1}{ac_h}\vec{a}_1 + \frac{n_2}{ac_h}\vec{a}_2 \tag{1a}$$

$$\hat{t} = \frac{n_1 + 2n_2}{\sqrt{3}ac_h}\vec{a}_1 + \frac{2n_1 + n_2}{\sqrt{3}ac_h}\vec{a}_2 \tag{1b}$$

solving for $\vec{a}_1$ and $\vec{a}_2$, we find that:

$$\vec{a}_1 = \frac{\sqrt{3}a}{2d}n_2\hat{t} + \frac{a}{2d}(2n_1 + n_2)\hat{c} \tag{2a}$$

$$\vec{a}_2 = -\frac{\sqrt{3}a}{2d}n_1\hat{t} + \frac{a}{2d}(2n_2 + n_1)\hat{c} \tag{2b}$$

If being $\vec{R}_{11}$, $\vec{R}_{12}$ and $\vec{R}_{13}$ are the position vectors for the atoms 11, 12 and 13, respectively, then

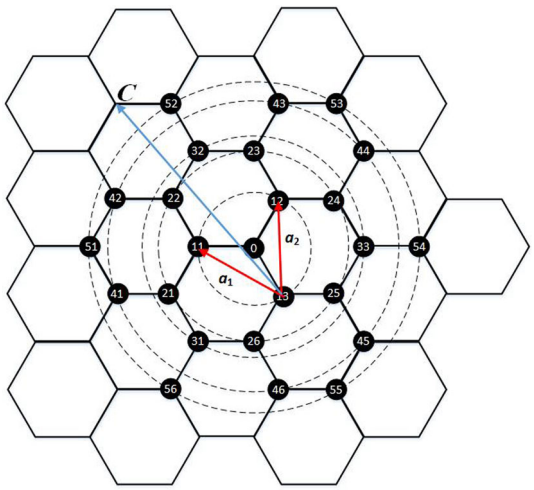

Fig. 1 Graphene lattice with the unit vectors $\vec{a}_1$ and $\vec{a}_2$ is illustrated. The nearest, second-, third-, fourth- and fifth-nearest neighboring atoms are also illustrated in unstrained lattice

$$\vec{r}_1 = \vec{R}_{11} - \vec{R}_0 = \frac{2\vec{a}_1 - \vec{a}_2}{3} \tag{3a}$$

$$\vec{r}_2 = \vec{R}_{12} - \vec{R}_0 = \frac{2\vec{a}_2 - \vec{a}_1}{3} \tag{3b}$$

$$\vec{r}_3 = \vec{R}_{13} - \vec{R}_0 = -(\vec{r}_1 + \vec{r}_2) \tag{3c}$$

Therefore,

$$\vec{r}_1 = \frac{a}{2\sqrt{3}c_h}(n_1 + 2n_2)\hat{t} + \frac{a}{2c_h}n_1\hat{c} \tag{4a}$$

$$\vec{r}_2 = -\frac{a}{2\sqrt{3}c_h}(2n_1 + n_2)\hat{t} + \frac{a}{2c_h}n_2\hat{c} \tag{4b}$$

From the continuum mechanics we know that if $\vec{r}_i = r_{it}\hat{t} + r_{ic}\hat{c}$, then

$$r_{it} \rightarrow r_{it}(1 + \varepsilon_t)(\text{tensile}) \tag{5a}$$

$$r_{ic} \rightarrow r_{ic} + r_{it}\tan(\theta)\ (\text{torsion}) \tag{5b}$$

where ε_t and θ are the percentage of tensile and angle of shear, respectively. Next, applying (5-a) and (5-b) on (4-a) and (4-b), we get:

$$\vec{r}_1 = \frac{a}{2\sqrt{3}c_h}(n_1 + 2n_2)(1 + \varepsilon_t)\hat{t} + \frac{a}{2c_h}\left[n_1 + \frac{(n_1 + 2n_2)\tan(\theta)}{\sqrt{3}}\right]\hat{c} \tag{6a}$$

$$\vec{r}_2 = -\frac{a}{2\sqrt{3}c_h}(2n_1 + 2n_2)(1 + \varepsilon_t)\hat{t} + \frac{a}{2c_h}\left[n_2 - \frac{(2n_1 + n_2)\tan(\theta)}{\sqrt{3}}\right]\hat{c} \tag{6b}$$

Since $\vec{a}_1 = \vec{r}_1 - \vec{r}_3$ and $\vec{a}_2 = \vec{r}_2 - \vec{r}_3$,

$$\vec{a}_1 = \frac{\sqrt{3}a(1 + \sigma_t)}{2d}n_2\hat{t} + \frac{a}{2d}\left[(2n_1 + n_2) + \sqrt{3}\tan(\theta)n_2\right]\hat{c} \tag{7a}$$

$$\vec{a}_2 = -\frac{\sqrt{3}a(1 + \sigma_t)}{2d}n_1\hat{t} + \frac{a}{2d}\left[(2n_2 + n_1) - \sqrt{3}\tan(\theta)n_1\right]\hat{c} \tag{7b}$$

Next, according to tight-binding model, we have:

$$\varphi_1(\boldsymbol{k}) = \frac{1}{\sqrt{N}}\sum_{n=1}^{N}\chi(\boldsymbol{r} - \boldsymbol{R}_{\mathrm{A}n})e^{i\boldsymbol{k}\cdot\boldsymbol{R}_{\mathrm{A}n}} \tag{8a}$$

$$\varphi_2(\boldsymbol{k}) = \frac{1}{\sqrt{N}}\sum_{n=1}^{N}\chi(\boldsymbol{r} - \boldsymbol{R}_{\mathrm{B}n})e^{i\boldsymbol{k}\cdot\boldsymbol{R}_{\mathrm{B}n}} \tag{8b}$$

$$\psi(\boldsymbol{k}) = c_1\varphi_1(\boldsymbol{k}) + c_2\varphi_2(\boldsymbol{k}) \tag{8c}$$

where φ_1 and φ_2 are the basis functions, $\boldsymbol{R}_{\mathrm{A}}$ and $\boldsymbol{R}_{\mathrm{B}}$ are the position vectors for lattice sites A and B, respectively, $\chi(\boldsymbol{r}\text{-}\boldsymbol{R}_{\mathrm{A}n})$ and $\chi(\boldsymbol{r}\text{-}\boldsymbol{R}_{\mathrm{B}n})$ are wave function of the p_z orbital at n'th atom at lattice sites A and B, respectively, and $\psi(\boldsymbol{k})$ is the wave function of the electron at the crystal lattice.

Starting from the tight-binding Hamiltonian and the overlap matrix (Reich et al. 2002):

$$\begin{vmatrix} H_{AA}(\boldsymbol{k}) - ES_{AA}(\boldsymbol{k}) & H_{AB}(\boldsymbol{k}) - ES_{AB}(\boldsymbol{k}) \\ H^*_{AB}(\boldsymbol{k}) - ES^*_{AB}(\boldsymbol{k}) & H_{AA}(\boldsymbol{k}) - ES_{AA}(\boldsymbol{k}) \end{vmatrix} = 0. \tag{9}$$

with

$$H_{AA}(\boldsymbol{k}) = \varphi_1|H|\varphi_1 = \frac{1}{N}\sum_{n=1}^{N}\sum_{n'=1}^{N} e^{i\boldsymbol{k}.(\boldsymbol{R}_{An}-\boldsymbol{R}_{An'})} \times \langle\chi(\boldsymbol{r}-\boldsymbol{R}_{An})|H|\chi(\boldsymbol{r}-\boldsymbol{R}_{An'})\rangle \tag{10a}$$

$$H_{AB}(\boldsymbol{k}) = \varphi_1|H|\varphi_2 = \frac{1}{N}\sum_{n=1}^{N}\sum_{n'=1}^{N} e^{i\boldsymbol{k}.(\boldsymbol{R}_{An}-\boldsymbol{R}_{Bn'})} \times \langle\chi(\boldsymbol{r}-\boldsymbol{R}_{An})|H|\chi(\boldsymbol{r}-\boldsymbol{R}_{Bn'})\rangle \tag{10b}$$

$$S_{AA}(\boldsymbol{k}) = \varphi_1|\varphi_1 = \frac{1}{N}\sum_{n=1}^{N}\sum_{n'=1}^{N} e^{i\boldsymbol{k}.(\boldsymbol{R}_{An}-\boldsymbol{R}_{An'})}\langle\chi(\boldsymbol{r}-\boldsymbol{R}_{An})|\chi(\boldsymbol{r}-\boldsymbol{R}_{An'})\rangle \tag{10c}$$

$$S_{AB}(\boldsymbol{k}) = \varphi_1|\varphi_2 = \frac{1}{N}\sum_{n=1}^{N}\sum_{n'=1}^{N} e^{i\boldsymbol{k}.(\boldsymbol{R}_{An}-\boldsymbol{R}_{Bn'})}\langle\chi(\boldsymbol{r}-\boldsymbol{R}_{An})|\chi(\boldsymbol{r}-\boldsymbol{R}_{Bn'})\rangle \tag{10d}$$

and

$$E = \frac{-(-2E_0+E_1) \pm \sqrt{(-2E_0+E_1)^2 - 4E_2E_4}}{2E_3} \tag{10e}$$

considering

$$E_0 = H_{AA}S_{AA} \tag{10f}$$

$$E_1 = S_{AB}H^*_{AB} + H_{AB}S^*_{AB} \tag{10g}$$

$$E_2 = H^2_{AA} - H_{AB}H^*_{AB} \tag{10h}$$

$$E_3 = S^2_{AA} - S_{AB}S^*_{AB} \tag{10i}$$

After solving (10a)–(10-d) regarding the fifth-nearest neighbor atoms, we get the following hopping parameters:

$$\varepsilon_{2p} = \langle\chi(\boldsymbol{r}-\boldsymbol{R}_0)|H|\chi(\boldsymbol{r}-\boldsymbol{R}_0)\rangle \tag{11a}$$

$$\gamma_1 = \langle\chi(\boldsymbol{r}-\boldsymbol{R}_{1j})|H|\chi(\boldsymbol{r}-\boldsymbol{R}_0)\rangle j = 1,2,3 \tag{11b}$$

$$s_1 = \langle\chi(\boldsymbol{r}-\boldsymbol{R}_{1j})|\chi(\boldsymbol{r}-\boldsymbol{R}_0)\rangle j = 1,2,3 \tag{11c}$$

$$\gamma_2 = \langle\chi(\boldsymbol{r}-\boldsymbol{R}_{2j})|H|\chi(\boldsymbol{r}-\boldsymbol{R}_0)\rangle\, j = 1,2,3,4,5,6 \tag{11d}$$

$$s_2 = \langle\chi(\boldsymbol{r}-\boldsymbol{R}_{2j})|\chi(\boldsymbol{r}-\boldsymbol{R}_0)\rangle j = 1,2,3,4,5,6 \tag{11e}$$

$$\gamma_3 = \langle\chi(\boldsymbol{r}-\boldsymbol{R}_{3j})|H|\chi(\boldsymbol{r}-\boldsymbol{R}_0)j\rangle = 1,2,3 \tag{11f}$$

$$s_3 = \langle\chi(\boldsymbol{r}-\boldsymbol{R}_{3j})|\chi(\boldsymbol{r}-\boldsymbol{R}_0)\rangle j = 1,2,3 \tag{11g}$$

$$\gamma_4 = \langle\chi(\boldsymbol{r}-\boldsymbol{R}_{4j})|H|\chi(\boldsymbol{r}-\boldsymbol{R}_0)\rangle j = 1,2,3,4,5,6 \tag{11h}$$

$$s_4 = \langle\chi(\boldsymbol{r}-\boldsymbol{R}_{4j})|\chi(\boldsymbol{r}-\boldsymbol{R}_0)\rangle j = 1,2,3,4,5,6 \tag{11i}$$

$$\gamma_5 = \langle\chi(\boldsymbol{r}-\boldsymbol{R}_{5j})|H|\chi(\boldsymbol{r}-\boldsymbol{R}_0)\rangle j = 1,2,3,4,5,6 \tag{11j}$$

$$s_5 = \langle\chi(\boldsymbol{r}-\boldsymbol{R}_{5j})|\chi(\boldsymbol{r}-\boldsymbol{R}_0)\rangle j = 1,2,3,4,5,6 \tag{11k}$$

where ε_{2p}, γ_1 to γ_5 and s_1 to s_5 can be found in Ref. (Han et al. 2010). We know that in the presence of mechanical strain, the hopping parameters change. So, because the distances are not the same as the non-strained lattice, in (11-b)–(11-k), we are faced with the parameters γ_{1j}, s_{1j} ($j = 1, 2, 3$), γ_{2j}, s_{2j} ($j = 1, \ldots, 6$), γ_{3j}, s_{3j} ($j = 1, 2, 3$), γ_{4j}, s_{4j} ($j = 1, \ldots, 6$) and γ_{5j}, s_{5j} ($j = 1, 2, 3$). But, because the distance between these atoms to the central atom (atom 0 in Fig. 1) compared with the nearest neighbor atoms to the central atom is far enough, we only consider the variations of the nearest neighbor parameters and assume that the variations of the remaining hopping parameters due to the strain is negligible. Therefore,

$$E_0 = \left[\varepsilon_{2p} + \gamma_2 u(\boldsymbol{k}) + \gamma_5 u(2k_1 - k_2, k_1 - 2k_2)\right] \times \left[1 + s_2 u(\boldsymbol{k}) + s_5 u(2k_1 - k_2, k_1 - 2k_2)\right] \tag{12a}$$

$$\begin{aligned} E_1 =& f_{s\gamma}(\boldsymbol{k}) + 2s_3\gamma_3 f(2\boldsymbol{k}) \\ &+ 2s_4\gamma_4[6 + u(\boldsymbol{k}) + u(2\boldsymbol{k}) + u(3\boldsymbol{k}) + t(\boldsymbol{k})] \\ &+ (s_3\gamma_4 + s_4\gamma_3)[g(\boldsymbol{k}) + u(2k_1 - k_2, k_1 - 2k_2) + t(\boldsymbol{k})] \\ &+ s_3 g_\gamma(\boldsymbol{k}) + \gamma_3 g_s(\boldsymbol{k}) + s_4\{(\gamma_{11} + \gamma_{12} + \gamma_{13})[u(\boldsymbol{k}) \\ &+ u(2\boldsymbol{k}) + u(2k_1 - k_2, k_1 - 2k_2)] \\ &- \left[u_\gamma(\boldsymbol{k}) + u_\gamma(2\boldsymbol{k}) + u_\gamma(2k_1 - k_2, k_1 - 2k_2)\right]\} \\ &+ \gamma_4\{(s_{11} + s_{12} + s_{13})[u(\boldsymbol{k}) + u(2\boldsymbol{k}) \\ &+ u(2k_1 - k_2, k_1 - 2k_2)] - [u_s(\boldsymbol{k}) + u_s(2\boldsymbol{k}) \\ &+ u_s(2k_1 - k_2, k_1 - 2k_2)]\} \end{aligned} \tag{12b}$$

$$\begin{aligned} E_2 =& \left[\varepsilon_{2p} + \gamma_2 u(\boldsymbol{k}) + \gamma_5 u(2k_1 - k_2, k_1 - 2k_2)\right]^2 \\ &- \{f_\gamma(\boldsymbol{k}) + \gamma_3 g_\gamma(\boldsymbol{k}) + \gamma_4[(\gamma_{11} + \gamma_{12} + \gamma_{13})(u(\boldsymbol{k}) \\ &+ u(2\boldsymbol{k}) + u(2k_1 - k_2, k_1 - 2k_2)) \\ &- \left(u_\gamma(\boldsymbol{k}) + u_\gamma(2\boldsymbol{k}) + u_\gamma(2k_1 - k_2, k_1 - 2k_2)\right)] \\ &+ \gamma_3^2 f(2\boldsymbol{k}) + \gamma_3\gamma_4[g(\boldsymbol{k}) + u(2k_1 - k_2, k_1 - 2k_2) + t(\boldsymbol{k})] \\ &+ \gamma_4^2[6 + u(\boldsymbol{k}) + u(2\boldsymbol{k}) + u(3\boldsymbol{k}) + t(\boldsymbol{k})]\} \end{aligned} \tag{12c}$$

$$\begin{aligned} E_3 =& [1 + s_2 u(\boldsymbol{k}) + s_5 u(2k_1 - k_2, k_1 - 2k_2)]^2 \\ &- \{f_s(\boldsymbol{k}) + s_3 g_s(\boldsymbol{k}) + s_4[(s_{11} + s_{12} + s_{13})(u(\boldsymbol{k}) + u(2\boldsymbol{k}) \\ &+ u(2k_1 - k_2, k_1 - 2k_2)) - (u_s(\boldsymbol{k}) + u_s(2\boldsymbol{k}) \\ &+ u_s(2k_1 - k_2, k_1 - 2k_2))] + s_3^2 f(2\boldsymbol{k}) \\ &+ s_3 s_4[g(\boldsymbol{k}) + u(2k_1 - k_2, k_1 - 2k_2) + t(\boldsymbol{k})] \\ &+ s_4^2[6 + u(\boldsymbol{k}) + u(2\boldsymbol{k}) + u(3\boldsymbol{k}) + t(\boldsymbol{k})]\} \end{aligned} \tag{12d}$$

The above axillary functions ($u(\boldsymbol{k})$, $f(\boldsymbol{k})$, $f_{s\gamma}(\boldsymbol{k})$, $f_\gamma(\boldsymbol{k})$, $f_s(\boldsymbol{k})$, $g_\gamma(\boldsymbol{k})$, $g_s(\boldsymbol{k})$, $g(\boldsymbol{k})$, $t(\boldsymbol{k})$) are defined in Appendix. If $= k_t\hat{\boldsymbol{t}} + k_c\hat{\boldsymbol{c}}$, then in case of uniaxial strain, the limits of k_t are given by $-\frac{\pi}{|\boldsymbol{T}|} \le k_t \le \frac{\pi}{|\boldsymbol{T}|}$, where $\boldsymbol{T}$ is the 1D lattice

vector length. The number of atoms in the 1D unit cell does not change in the presence of uniaxial strain and so the range of m does not change from the undeformed case ($m = 0, 1, 2, \ldots, N$ where N is the number of hexagons in the 1D unit cell). In the case of torsion, the number of atoms in the 1D unit cell and $\mathbf{T}$ can be large. The corresponding span of $k_t = \boldsymbol{k} \cdot \hat{\boldsymbol{t}}$ is then small compared to the undeformed tube and the range of m is commensurate with the number of atoms in the 1D unit cell (Yang et al. 1999).

As can be seen in (12-a)–(12-d), the third harmonic of $\boldsymbol{k}$ is now in our equation in addition to the first and the second ones, while the nearest neighbor approximation only regard the first harmonic, and the third-nearest neighbor approximation regard the first and the second harmonics of the wave vector $\boldsymbol{k}$. In Eqs. (12-a)–(12-d) γ_{1j} is given by (Harrison 1989): $\frac{\gamma_{1j}}{\gamma_1} = \left(\frac{a_{C-C}}{r_{1j}}\right)^2$ where $r_{1j} = \left|\boldsymbol{r}_{1j} - \boldsymbol{R}_0\right|$, and $\boldsymbol{r}_{1j}$ being the position vector of atom $1j$. Now, s_{1j} can be acquired by means of the following:

$$\frac{\gamma_{1j}}{\gamma_1} = \frac{\chi(\boldsymbol{r} - \boldsymbol{R}_0)|H|\chi(\boldsymbol{r} - \boldsymbol{R}_{1j})\text{with strain}}{\chi(\boldsymbol{r} - \boldsymbol{R}_0)|H|\chi(\boldsymbol{r} - \boldsymbol{R}_{1j})\text{without strain}} = \frac{\chi(\boldsymbol{r} - \boldsymbol{R}_0)|\chi(\boldsymbol{r} - \boldsymbol{R}_{1j})\text{with strain}}{\chi(\boldsymbol{r} - \boldsymbol{R}_0)|\chi(\boldsymbol{r} - \boldsymbol{R}_{1j})\text{without strain}} = \frac{s_{1j}}{s_1} \tag{13}$$

for small percentage of strain. Now that we worked out E_0, E_1, E_2, E_3, in order to use (10-e) for SWCNTs it must be considered with Born–von Karman boundary condition:

$$\boldsymbol{k} \cdot \boldsymbol{C} = 2\pi m \tag{14}$$

where m is a natural number. In order to calculate the DOS, we have to use the following equation:

$$n(E) = \frac{2}{l}\sum_m \int \delta(k - k_q)\left|\frac{\partial E}{\partial k}\right|^{-1} \mathrm{d}k \tag{15}$$

where $n(E)$ is $\frac{\partial N(E)}{\partial E}$ ($N(E)$ is the total number of states per unit cell below a given energy E) and l is the length of the one-dimensional Brillouin zone that is equal to the total area of the first Brillouin zone divided by the interline spacing; we can write the DOS per carbon atom $\rho(E)$ as (Mintmire and White 1998):

$$\rho(E) = \frac{n(E)}{2} = \frac{4}{l}\sum_{\text{all } k' \text{ son all subbands having the enegy } E}\left|\frac{\partial E}{\partial k_{||}}\right|^{-1} \tag{16}$$

where $k|$ are the wave vectors which meet condition (14).

3 Applications and Results

In this section, we use our method to estimate the band gap and the density of states for a number of chiral vectors. Then, we compare our results with the previous models of tight-binding approximation. We also examine the density of states under applied strains.

Illustrated in Fig. 2 is the band gap of a number of chiral vectors under a small percentage of uniaxial strain. As can be seen in the figure, in nonzero strain the band gap values change for all three tight-binding approximations. For most of the cases, the band gap varies along a straight line which agrees with that of (Yang et al. 1999) and (Pakkhesal and Ghayour 2010). The sign of the slope of such lines is determined by $(n_1–n_2)$ *mod3* rule for uniaxial strain, and its magnitude depends on the chiral angle as is given in (Yang et al. 1999). Nonetheless, in some chiral vectors (like (8,6)), there is a gradual reversal in the slope of band gap variations which is because of the displacement of sub-bands at the band edge which is well discussed in (Pakkhesal and Ghayour 2010). Also, in this figure it can be seen that the values which are calculated using 3-NN-TB are in better agreement with that of 5-NN-TB approximation.

Illustrated in Fig. 3 are the values of band gap variations due to the shear strain. As can be seen, in most of the cases there is better agreement between the 3-NN-TB and the 5-NN-TB values. Besides, in a small number of chiral vectors, as the percentage of torsional strain increases, the 5-NN-TB shows an indirect band gap, e.g., (5,5) at 5% of strain.

As is shown in Fig. 3, in some of the cases, the three methods agree in linear relationship between the angle of shearing strain and the band gap variations for small percentage of strain like (5,5), (8,0), but in some other ones like (7,0) and (7,6) there are some deviations from the linear behavior of band gap versus shear, which is well emphasized by 5-NN-TB approximation. In a small number of cases like those of (8,6) and (5,4) there are approximately no linear relationships, which implies nonlinear displacements of the sub-bands of the band edges.

In linear cases, for chiral tubes, $|\mathrm{d}E_g/\mathrm{d}(\text{degrees of shear strain})|$ decreases with increase in chiral angle and the slope of $\mathrm{d}E_g/\mathrm{d}(\text{degrees of shear strain})$ follows $(n_1–n_2)$ *mod3* rule which agrees with that of (Yang et al. 1999).

Illustrated in Figs. 4 and 5 are the variations of the DOS vs. uniaxial strain and vs. degrees of shear, respectively. These figures are plotted for the chiral vectors (7,0) and (8,0). In this, figures (a), (b) are calculated with the nearest neighbor tight binding, (c), (d) with 3-NN-TB and (e), (f) with 5-NN-TB. It is worth mentioning that the point of discontinuities happened due to the value of infinity from our calculating software. As is illustrated in Fig. 4, the three methods agree that as a result of the application of uniaxial strain, DOS increases at band edges with increasing percentage of strain for (7,0) and decreases with increasing strain at band edges for (8,0). The points of

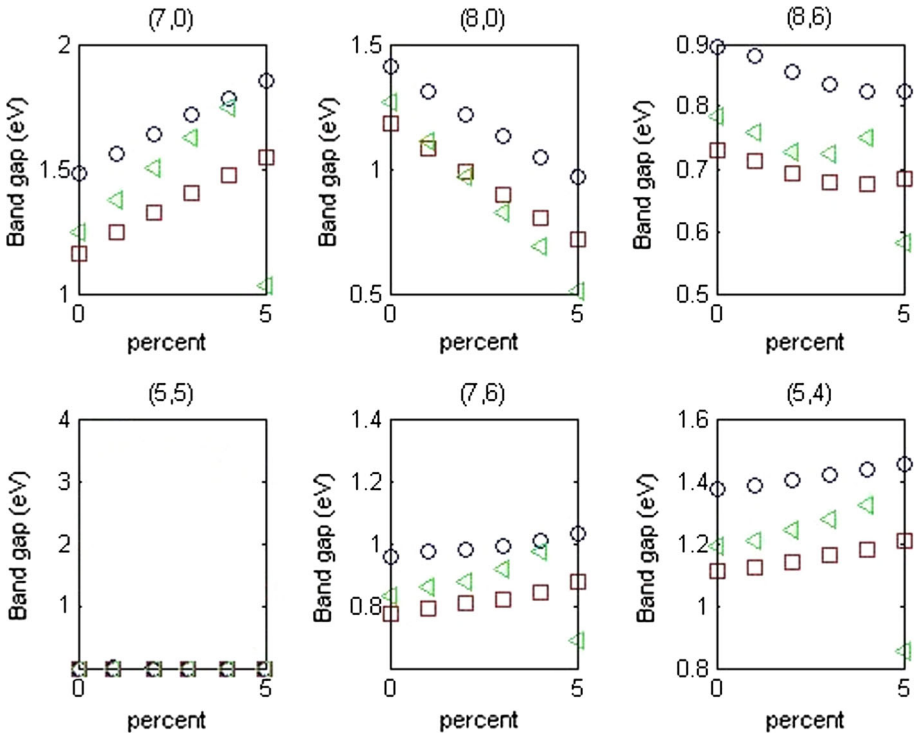

Fig. 2 Band gap variations of a number of SWCNTs with different chiral vectors for zero to 5% of tensile strain are depicted. The values are calculated according to the nearest neighbor (*circles*), third-nearest neighbor (*squares*) and fifth-nearest neighbor (*triangles*) tight-binding approximations

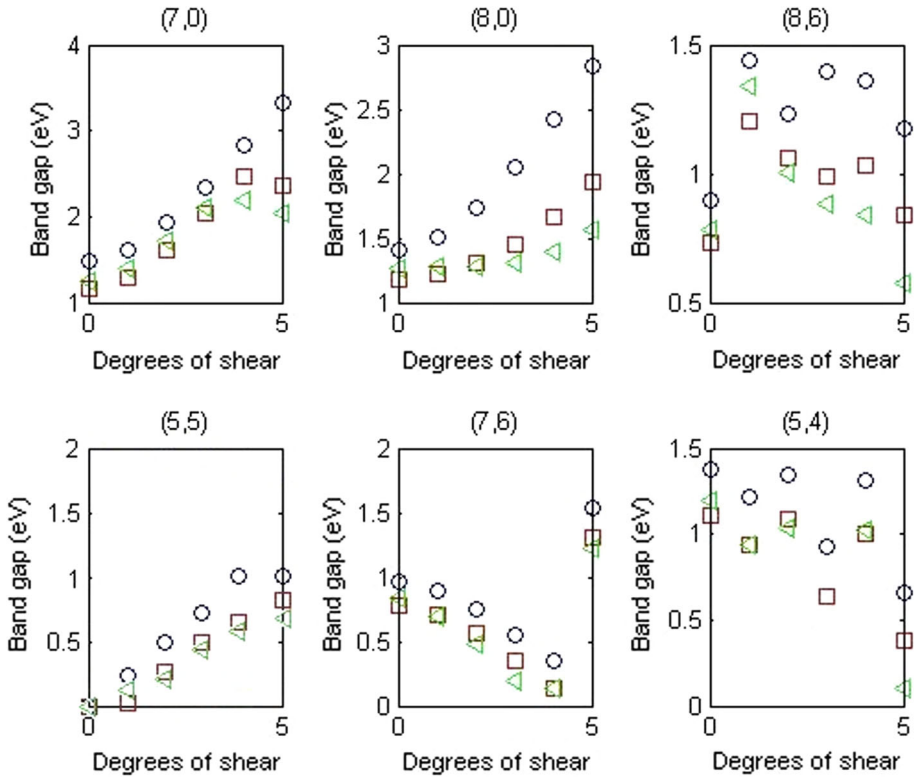

Fig. 3 Band gap variations of a number of SWCNTs with different chiral vectors, for zero to 5 degrees of shear strain, are depicted. The values are calculated according to the nearest neighbor (*circles*), third-nearest neighbor (*squares*) and fifth-nearest neighbor (*triangles*) tight-binding approximations

singularities correspond to the van Hove singularities which occur near the corners of hexagonal Brillouin zone of the graphene lattice.

Also, Fig. 5 depicts the DOS vs. degrees of shear using the three tight-binding methods. Figure 5a, b shows that, in spite of the gap values, the DOS at band edges decreases

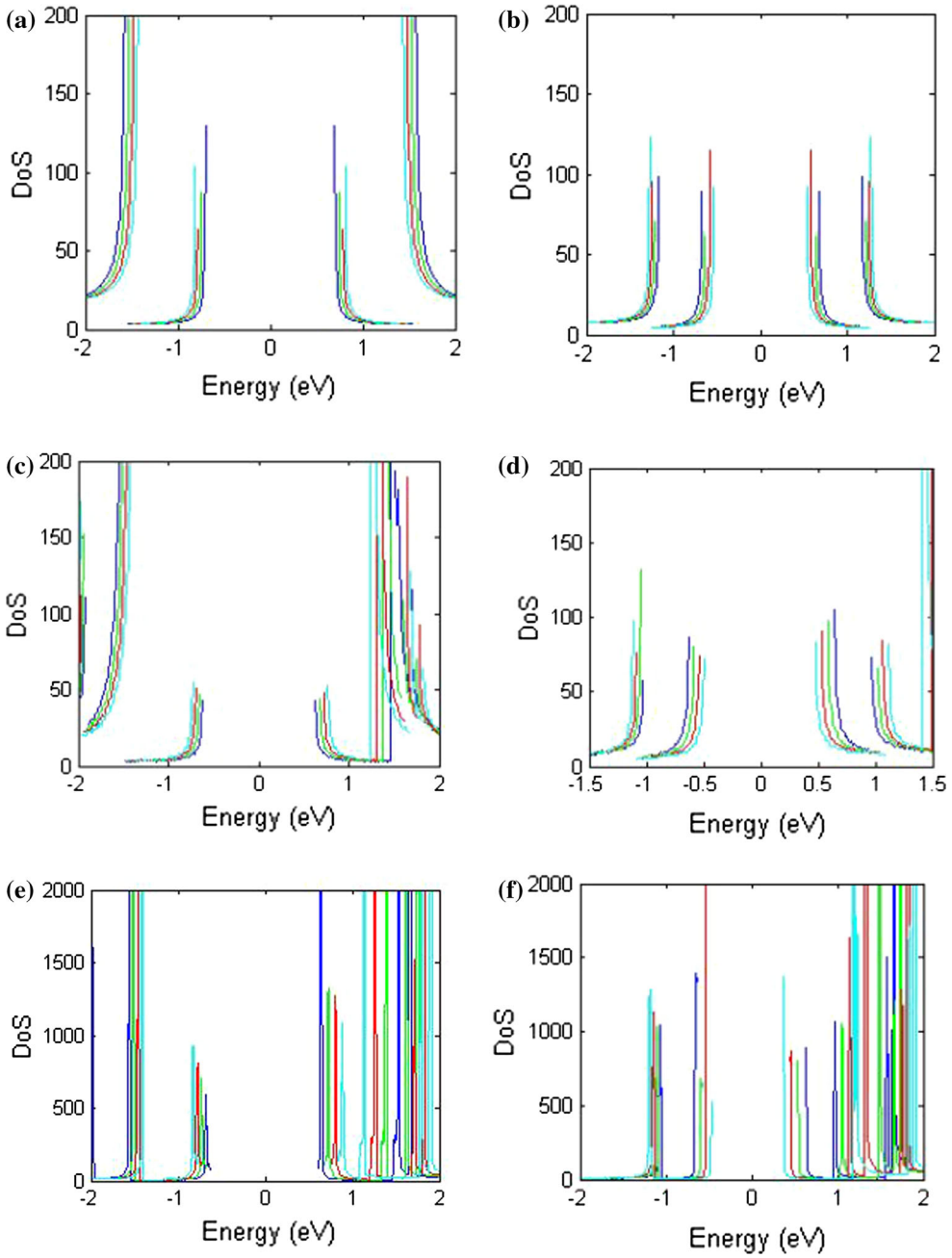

Fig. 4 Variations of the DOS (per carbon atom) vs. uniaxial strain for (7,0), calculated using the nearest neighbor tight binding (**a**), 3-NN-TB (**c**) and 5-NN-TB (**e**) and for (8,0) calculated using the nearest neighbor tight binding (**b**), 3-NN-TB (**d**) and 5-NN-TB (**f**). Also in this figure, *blue curved lines* show 0%, *green* 1%, *red* 2% and *cyan* 3% of tensile

with increasing strain according to the nearest neighbor tight-binding model.

Besides, it shows that as the strain increases the singularities at the band edges vanish. However, the 3-NN-TB as in Fig. 5b, c and 5-NN-TB as in Fig. 5e, f does not show a serious variation of the DOS with shearing strain.

4 Conclusion

In this article, we investigated the response of three tight-binding models to two types of mechanical deformation, i.e., uniaxial and torsional strains. Initially, we developed a perturbed fifth-nearest neighbor tight-binding model using the original unperturbed fifth-nearest neighbor model.

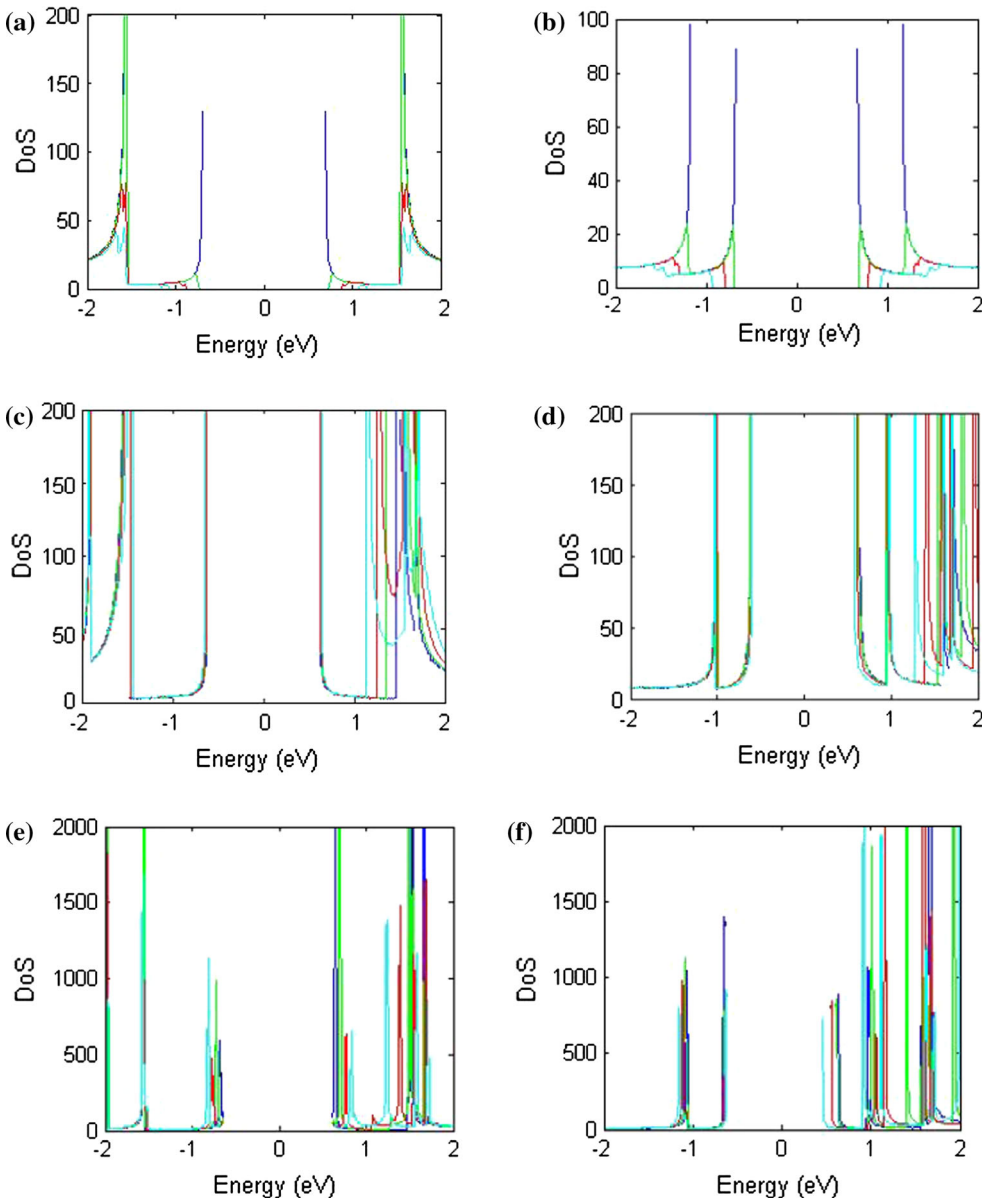

Fig. 5 Variations of the DOS (per carbon atom) vs. degrees of shearing strain for (7,0), calculated using the nearest neighbor tight binding (**a**), 3-NN-TB (**c**) and 5-NN-TB (**e**) and for (8,0) calculated using the nearest neighbor tight binding (**b**), 3-NN-TB (**d**) and 5-NN-TB (**f**). Also in this figure, *blue curved lines* show 0 degrees, *green* 1 degree, *red* 2 degrees and *cyan* 3 degrees of tensile

Next, we applied our 5-NN-TB model to investigate the band gap and DOS variations of a number of SWCNT and compared the values with the nearest and the third-nearest neighbor tight-binding approximations.

Comparison of the three methods shows that while the 3-NN-TB and 5-NN-TB values are in better agreement, there are differences in the acquired values of the three methods and because the 5-NN-TB model considers the fourth and the fifth-nearest neighbors in addition to the first, second and third ones, it yields more exact values than its nearest and the third-nearest counterparts as is shown in (Han et al. 2010). The results of this paper enable us to analytically investigate the effects of the mentioned types of strain on the band gap and the DOS of SWCNTs while maintaining the acceptable levels of accuracy.

Appendix

$$u(\vec{k}) = 2\cos\left(\vec{k}\cdot\vec{a}_1\right) + 2\cos\left(\vec{k}\cdot\vec{a}_2\right) + 2\cos\left[\vec{k}\cdot(\vec{a}_2-\vec{a}_1)\right] \tag{A1}$$

$$f(\vec{k}) = 3 + u(\vec{k}) \tag{A2}$$

$$f_{s\gamma}\left(\vec{k}\right) = 2(s_{11}\gamma_{11}+s_{12}\gamma_{12}+s_{13}\gamma_{13}) + 2(s_{11}\gamma_{13}+s_{13}\gamma_{11})\cos(\vec{k}\cdot\vec{a}_1) + 2(s_{12}\gamma_{13}+s_{13}\gamma_{12})\cos(\vec{k}\cdot\vec{a}_2) + 2(s_{11}\gamma_{02}+s_{12}\gamma_{11})\cos[\vec{k}.(\vec{a}_2-\vec{a}_1)] \tag{A3}$$

$$f_{\gamma\gamma}(\vec{k}) = \gamma_{11}^2+\gamma_{12}^2+\gamma_{13}^2+2\gamma_{11}\gamma_{13}\cos(\vec{k}\cdot\vec{a}_1) + 2\gamma_{12}\gamma_{13}\cos(\vec{k}\cdot\vec{a}_2) + 2\gamma_{11}\gamma_{12}\cos[\vec{k}\cdot(\vec{a}_2-\vec{a}_1)] \tag{A4}$$

$$f_{ss}\left(\vec{k}\right) = s_{11}^2 + s_{12}^2 + s_{13}^2 + 2s_{11}s_{13}\cos\left(\vec{k}\cdot\vec{a}_1\right) + 2s_{12}s_{13}\cos\left(\vec{k}\cdot\vec{a}_2\right) + 2s_{11}s_{12}\cos\left[\vec{k}\cdot(\vec{a}_2-\vec{a}_1)\right] \quad \text{(A5)}$$

$$u_\gamma\left(\vec{k}\right) = 2\gamma_{12}\cos(\vec{k}\cdot\vec{a}_1) + 2\gamma_{11}\cos(\vec{k}\cdot\vec{a}_2) + 2\gamma_{13}\cos[\vec{k}\cdot(\vec{a}_2-\vec{a}_1)] \quad \text{(A6)}$$

$$u_s(\vec{k}) = 2s_{12}\cos(\vec{k}\cdot\vec{a}_1) + 2s_{11}\cos(\vec{k}\cdot\vec{a}_2) + 2s_{13}\cos[\vec{k}\cdot(\vec{a}_2-\vec{a}_1)] \quad \text{(A7)}$$

$$g_\gamma\left(\vec{k}\right) = 2u_\gamma\left(\vec{k}\right) + u_\gamma(k_1-2k_2, 2k_1-k_2) \quad \text{(A8)}$$

$$g_s\left(\vec{k}\right) = 2u_s\left(\vec{k}\right) + u_s(k_1-2k_2, 2k_1-k_2) \quad \text{(A9)}$$

$$t(\boldsymbol{k}) = u(3k_1-k_2, k_1+2k_2) + u(3k_2-k_1, 2k_1+k_2) \quad \text{(A10)}$$

References

Bahari A, Amiri M (2012) Simulation study of the electron and hole transport in a CNTFET. Commun Theor Phys 59:121–124

Han YJ, Wei-Wei J, Er-Qiang L, Tian-Sung P, Yuan-Yuan Z, Hui W (2010) Fifth-nearest-neighbor tight-binding description of electronic structure of graphene. Commun Theor Phys 53:1172–1176

Harrison WA (1989) Electronic structure and the properties of solids. Dover, New York

Mintmire JW, White CT (1998) Universal density of states for carbon nanotubes. Phys Rev Lett 81:2506–2509

Pakkhesal M, Ghayour R (2010) Mechanically changed band gap of single walled carbon nanotube: a third neighbor tight-binding approach. Cent Eur J Phys 8:304–311

Reich S, Maultzsch J, Thomsen C (2002) Tight-binding description of graphene. Phys Rev B 66:0354121–0354125

Saito R, Fujita M, Dresselhaus G, Dresselhaus MS (1992) Electronic structure of chiral graphene tubules. Appl Phys Lett 60:2204–2206

Sivasathya S, Thiruvadigal DJ (2013) The effects of defects on electron transport in metallic single wall carbon nanotubes. NanoSys Phys Chem Math 4:405–408

Souier T, Maragliano C, Stefancich M, Chiesa M (2013) How to achieve high electrical conductivity in aligned carbon nanotube polymer composites. Carbon 64:150–157

Wan-Sheng S (2013) Electronic and structural properties of carbon nanotubes modulated by external strain. J Appl Phys 113:2443081–2443086

White CT, Robertson DH, Mintmire JW (1993) Helical and rotational symmetries of nanoscale graphitic tubules. Phys Rev B 47:5485–5488

Yang L, Anantram MP, Han J, Lu JP (1999) Band-gap change of carbon nanotubes: effect of small uniaxial and torsional strain. Phys Rev B 60:13874–13878

Zang M (2005) Band theory of single-walled carbon nanotubes. IEEE Trans Nanotechnol 4:452–459